Injection of charge nanostructures into insulators

Hans-Joachim Fitting, N. Cornet, Matthieu Touzin, D. Goeuriot, Christelle Guerret-Piecourt, Denyse Juvé, Daniel Tréheux

Injection of charge nanostructures into insulators

H.-J. Fitting [a,*], N. Cornet [b], M. Touzin [c], D. Goeuriot [b], C. Guerret-Piécourt [d], D. Juvé [d], D. Tréheux [d]

[a] *Institute of Physics, University of Rostock, Universitaetsplatz 3, D-18051 Rostock, Germany*
[b] *Ecole Nationale Supérieure des Mines, 158 cours Fauriel, F-42023 Saint-Etienne, France*
[c] *Université de Sciences et Technologies de Lille, F-59655 Villeneuve d'Ascq, France*
[d] *Ecole Centrale de Lyon, 36 avenue Guy de Collongue, F-69134 Ecully, France*

The electron beam induced selfconsistent charge transport in insulators is described by means of an electron-hole flight–drift model FDM and an iterative computer simulation. Ballistic secondary electrons and holes, their attenuation and drift, as well as their recombination, trapping, and detrapping are included. Thermal and field-enhanced detrapping are described by the Poole–Frenkel effect.

As a main result the time dependent secondary electron emission rate $\sigma(t)$ and the spatial distributions of currents $j(x, t)$, charges $\sigma(x, t)$, field $F(x, t)$, and potential $V(x, t)$ are obtained. The spatial charge distributions with depth show a quadropolar plus–minus–plus–minus structure in nanometer dimensions.

1. Introduction

In electron microscopy like scanning electron microscopy (SEM) or Auger electron spectroscopy (AES), electron energy loss spectroscopy (EELS) etc., the prediction of electrical charging is essentially to interpret the measurements, see e.g. [1]. Moreover, charging of non-conductive samples has to be known in order to manage applications such as functional layers and in nanotechnology, [2].

A great number of experimental and theoretical investigations have been published on the charging of insulators due to electron bombardment and the related secondary electron emission (SEE). Only for short pulse irradiation, target charging is prevented and the real charging-free secondary electron emission yield $\sigma(E_0)$ as a function of the primary electron energy E_0 can be measured as well as has

* Corresponding author. Tel.: +49 381 498 6760.
E-mail address: hans-joachim.fitting@uni-rostock.de (H.-J. Fitting).

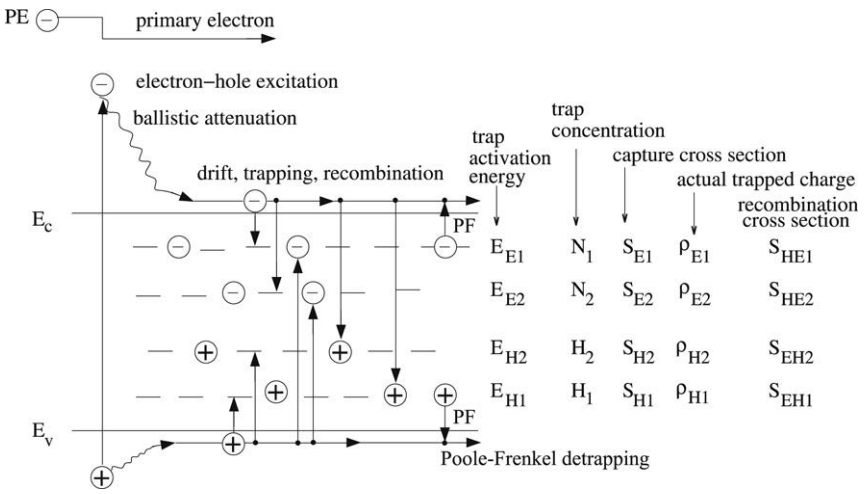

Fig. 1. Scheme of the flight–drift model (FDM) including the excitation of ballistic electrons and holes, their flight and attenuation, followed by drift or diffusion, trapping or recombination and/or Poole–Frenkel (PF) release, see Eqs. (3)–(5).

been determined theoretically for various insulators [3,4]. However, the charging behaviour under permanent electron irradiation is not yet fully understood and the stationary final state is still very complex to describe. Indeed, the total yield approach ($\sigma \gtrless 1$) is often used to predict the sign ($\pm$) of charging in the case of stationary electron irradiation, but experimental results are not fully consistent with these predictions [1,5].

It is of importance to determine the types of theory that have been led to enlighten this phenomenon. One of the first attempts was the planar (1-dimensional) selfconsistent charging simulation of our co-author (HJF) already in 1979, [6], later improved on in Refs. [7–10]. These authors use field-dependent attenuation lengths $\lambda(F)$ for the ballistic transport of electrons and holes which had been found experimentally by means of electron beam induced current (EBIC) measurements.

The present paper will extend the model of ballistic electron and hole transport to drift processes, recombination and charge trapping processes, as has already been shown in Ref. [10]. Thus, spatial charge profiles in nanoscale dimensions are built up in insulating samples. The results will be presented in particular for silica SiO_2 similar to what has been shown earlier for alumina Al_2O_3 [8–10], but can be easily adapted to any insulator using the relevant material data available in the literature.

2. Theoretical background

The various processes of electron beam charge injection into a dielectric target are demonstrated in Fig. 1. Incident electrons (so-called primary electrons PE) with initial energy E_0 and current density j_0 penetrate the insulator target up to the maximum range $R(E_0)$. The injection of primary electrons (PE) and their creation of secondary electrons (SE) and holes (H) are very similar for silica SiO_2 and alumina Al_2O_3 as we have described already in Ref. [10]. The resulting PE current density in dependence on the target depth x and the PE initial energy E_0 was found:

$$j_{PE}(x, E_0) = j_0(1 - \eta_B) \exp\left[-4.605 \left(\frac{x}{R(E_0, Z)}\right)^{p(Z)}\right], \tag{1}$$

with j_0 as impinging PE current density and the material parameters for SiO_2 and Al_2O_3: $\eta_B \approx 0.2$ the backscattering coefficient, $p = 2$ the transmission exponent. An appropriate formula for the maximum range $R(E_0)$ of electrons reached by 1% of PE in dependence on their initial energy E_0 was deduced from experimental data in [11] for the relevant energy region $1 < E_0 \leq 30$ keV with:

$$R_{SiO_2} = 33.7\ (E_0/\text{keV})^{1.55} \tag{2a}$$

$$R_{Al_2O_3} = 28.7\ (E_0/\mathrm{keV})^{1.55} \tag{2b}$$

where R is given in nm, and the electron beam energy E_0 should be inserted in keV.

The Flight–Drift Model (FDM) with the scattering and straggling of primary electrons (PE), their excitation of secondary electrons (SE) and holes (SH), their ballistic flight as ballistic electrons (BE) and holes (BH), respectively, their attenuation and drift as drifting electrons (DE) and holes (DH) in selfconsistent fields, followed by recombination or trapping in and/or Poole–Frenkel detrapping from localized states (traps) is presented schematically in Fig. 1 and has been described comprehensively in our previous paper [10]. All these processes are included in the following Eq. (3) for drifting electrons (DE) in reverse (R) direction towards the surface and transmission (T) directions into the sample volume (bulk). The respective attenuation probabilities of ballistic electrons over the depth element Δx in reverse (R) and transmission (T) direction in the presence of an electric field F are described by:

$$W_{\mathrm{EFT}}^{\mathrm{EFR}} = \exp\left[-\frac{\Delta x}{\lambda_{E,0}\exp(\pm\beta_E F)}\right] \tag{3}$$

where $\lambda_{E,0}$ is the mean attenuation length and β_E its field enhancement coefficient approved already in [6,7]. Thus the expressions $[1 - W]$ always express the generation of attenuated, i.e. diffusing and drifting electrons.

$$\begin{aligned} j_{\mathrm{DET}}^{\mathrm{DER}}(x) = \{ & j_{\mathrm{DET}}^{\mathrm{DER}}(x \pm \Delta x) \\ & + \text{convection} \\ & + [j_{\mathrm{BER}}(x)[1 - W_{\mathrm{EFR}}(x)] + j_{\mathrm{BET}}(x)[1 - W_{\mathrm{EFT}}(x)] \\ & + \text{generation by ballistic attenuation} \\ & + \varrho_{\mathrm{E1}}(x) W_{\mathrm{E1PF}} + \varrho_{\mathrm{E2}}(x) W_{\mathrm{E2PF}}] \times F_{\mathrm{E}}(x)\} \\ & + \text{detrapping by Poole–Frenkel effect} \\ & \times \underbrace{\exp\left[-\left(N_1 - \frac{\varrho_{E1}}{e_0}\right) S_{\mathrm{E1}} \Delta x\right]}_{W_{\mathrm{E1}}} \cdot \underbrace{\exp\left[-\left(N_2 - \frac{\varrho_{E2}}{e_0}\right) S_{\mathrm{E2}} \Delta x\right]}_{W_{\mathrm{E2}}} \\ & \times \text{trapping probability in shallow}^{(1)} \text{and deep}^{(2)} \text{states} \\ & \times \underbrace{\exp\left[-\frac{\varrho_{H1}}{e_0} S_{\mathrm{EH1}} \Delta x\right]}_{W_{\mathrm{EH1}}} \cdot \underbrace{\exp\left[-\frac{\varrho_{H2}}{e_0} S_{\mathrm{EH2}} \Delta x\right]}_{W_{\mathrm{EH2}}} \\ & \times \text{recombination probability with holes.} \end{aligned} \tag{4}$$

Here the first convection term describes incoming and outgoing drifting electrons in the depth element Δx; the second generation term presents the sources of drifting electrons by attenuated (exhausted) ballistic electrons; the third (detrapping) term is given by the Poole–Frenkel release of electrons from traps, presenting also a source of drifting electrons. The Poole–Frenkel [12] release of charges (here electrons) from traps E_{n} is given by

$$W_{\mathrm{EPF}} = f_{\mathrm{E}} \exp\left[-\frac{E_{\mathrm{n}} - \Delta E_{\mathrm{PF}}}{kT}\right] \tag{5}$$

with trap barrier lowering ΔE_{PF} by an electric field F:

$$\Delta E_{\mathrm{PF}} = 2\left(\frac{e^3}{4\pi\epsilon_0\epsilon_r}\right)^{1/2} F^{1/2}. \tag{6}$$

The field factor $F_E(x)$ in Eq. (4) describes the anisotropy of all generated drifting electrons (DE) in the present electric field $F(x)$. Finally, as electron drains we see the trapping and recombination terms with trap concentrations N and actual charges ϱ as well as the respective cross sections S, all as

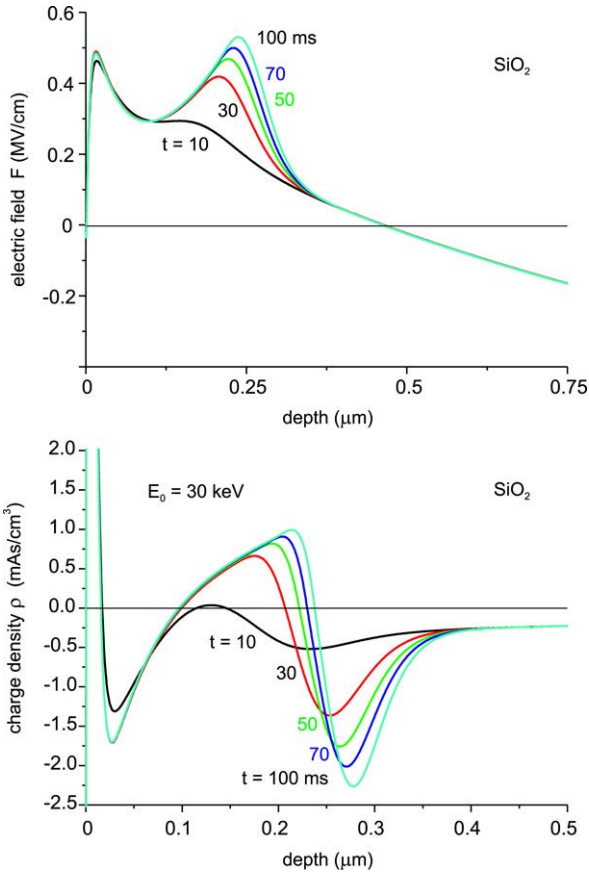

Fig. 2. Spatial charge $\rho(x,t)$ and field $F(x,t)$ distributions in bulk silica as a function of irradiation time t for an incident electron beam energy $E_0 = 30$ keV and current density $j_0 = 10^{-5}$ A/cm^2.

presented in Fig. 1. Of course, the current density equation $j_{\mathrm{DHT}}^{\mathrm{DHR}}$ for drifting holes (DH) looks adequate with the respective trapping parameters of holes, as already described in Refs. [9,10].

The resulting charges will be counted from the balance of trapping and detrapping: $\varrho(x,t) = -\varrho_{\mathrm{E1}} - \varrho_{\mathrm{E2}} + \varrho_{\mathrm{H1}} + \varrho_{\mathrm{H2}}$. On the other hand, we may account for the charges and the fields from the total current flux (divergences) too:

$$-\frac{\partial}{\partial x} j(x,t) = \frac{\partial \varrho(x,t)}{\partial t} = \epsilon_0 \epsilon_r \frac{\partial}{\partial t} \frac{\partial}{\partial x} F(x,t) \tag{7}$$

as has been already described in more detail in Ref. [9].

3. Results and discussion

The present selfconsistent transport and charging simulations have been performed for 3 mm thick (bulk) silica samples by means of material parameters given already in previous work [7, 10]. The charge $\rho(x)$ and field $F(x)$ distributions in dependence on electron beam irradiation time $t = (10 \ldots 100)$ ms ($E_0 = 30$ keV, $j_0 = 10^{-5}$ A/cm^2) are presented in Fig. 2. Beneath the surface, where especially the emerging secondary electrons are coming from, we see the built-up of a strong positive charge distribution with a center of gravity at about 2.5 nm. The positive field is increasing enforcing field-enhanced secondary electron emission (SEE) into the vacuum. The field

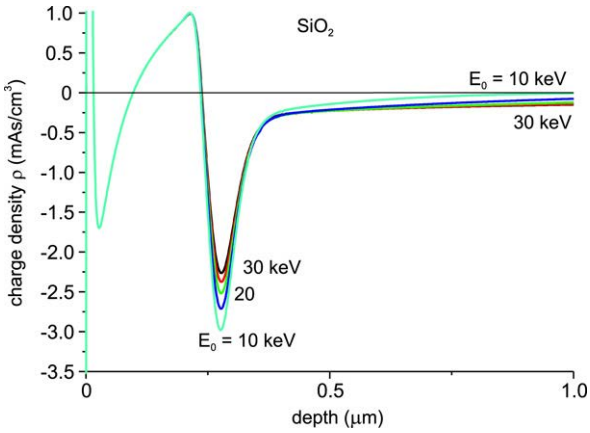

Fig. 3. Stationary spatial charge distributions $\rho(x)$ after saturation ($t > 100$ ms) for different incident electron beam energies E_0 and a constant current density $j_0 = 10^{-5}$ A/cm^2.

remains positive up to 0.4 μm sweeping electrons towards the surface and holes into the bulk. Then, beyond 0.5 μm, the field changes to negative values and keeps almost constant up to the support electrode at $x = d = 3$ mm. Due to the bipolar field distribution the drifting electrons and holes form a quadropolar charge distribution. The positive surface charge is due to emitted SE's and remaining holes. Then the positive field $F > 0$ is separating electrons towards the surface (negative) and holes into the bulk (positive). An opposite charge separation is obtained in the region with an opposite negative field $F < 0$: holes are swept in a direction to the surface and electrons into the bulk, finally resulting in the quadropolar charge distribution: plus–minus–plus–minus.

Here we should mention that all distributions, especially of $j_{\text{tot}}(x)$ and $\rho_{\text{tot}}(x)$, are shrunk towards the surface and do not reach the electron maximum range $R(E_0)$ in a remarkable extent as can be seen very evidently in the final stationary charge distributions in Fig. 3. The reason for that is given by the overall negative charging and the resulting negative surface potential V_0, as we see in Fig. 4, diminishing the actual landing energy of the electron beam $E_0' = E_0 + eV_0$ with $V_0 < 0$. A respective measurement proof has been made by recording the X-ray bremsstrahlung (BS) and its high energy threshold given by $h\nu_{\text{BS}} = E_0'$, see [8]. Another criterion for the final stationary state of charging is $j_{\text{tot}}(x, t) = \text{const}$, in bulk insulating samples it is $j_{\text{tot}}(x, t) = \text{const} = 0$ and $\sigma = 1$ as we see in the upper part of Fig. 4. Under these conditions no more charges will be stored and the final steady state is reached.

4. Conclusions

Electron beam irradiation and charge injection associated by selfconsistent charge transport in insulating samples are described by means of an electron-hole flight–drift model (FDM) implemented by an iterative computer simulation. Ballistic scattering and transport of secondary electrons and holes are followed by electron and hole drift, their possible recombination and/or trapping in shallow and deep traps. Furthermore a detrapping by the temperature- and field-dependent Poole–Frenkel effect becomes possible allowing even a charge hopping transport. As a main result the spatial distributions of currents $j(x, t)$, charges $\rho(x, t)$, electric field $F(x, t)$, and potential $V(x, t)$ are obtained in a selfconsistent procedure as well as the time dependent secondary electron emission rate $\sigma(t)$ and surface potential $V_0(t)$; both are experimentally accessible. For bulk full insulating samples the above quoted time-dependent distributions approach the final stationary state under the condition $j(x, t) = \text{const} = 0$ and $\sigma = 1$. Because of charging and a resulting high negative surface potential V_0 the electron beam is decelerated down to an actual landing energy $E_0' = E_0 + eV_0$ close to the energy E_{02} where $\sigma(E_0)$ approaches the value of unity. Generally we obtain a bipolar field distribution $F(x)$: a positive field near the surface and a negative one in the remaining bulk. Due to drift processes

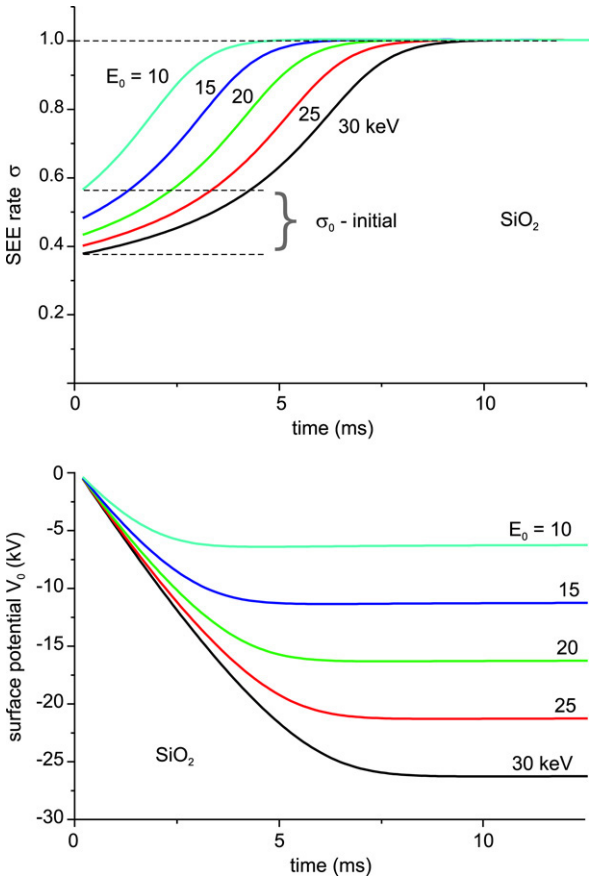

Fig. 4. Secondary electron emission rate σ and surface potential V_0 of a bulk (3 mm) silica target as a function of irradiation time t for different electron beam energies E_0 and a current density $j_0 = 10^{-5}$ A/cm^2.

we obtain opposite charge separations of electrons and holes leading in the opposite field regions to the quadropolar charge structure $\rho(x)$: plus–minus–plus–minus in nanoscale dimensions beneath the surface.

References

[1] J. Cazaux, J. Appl. Phys. 89 (2001) 8265.
[2] 4th International Conference on Electric Charges in Non-Conductive Materials, Le Vide: Science, Techniques et Applications, Vol. Special CSC'4, 2001.
[3] H. Seiler, Z. Angew. Phys. 22 (1967) 249.
[4] L. Reimer, Scanning Electron Microscopy, in: Springer Series in Optical Sciences, vol. 45, Berlin, 1985.
[5] A. Melchinger, S. Hofmann, J. Appl. Phys. 78 (1995) 6624.
[6] H.-J. Fitting, H. Glaefeke, W. Wild, M. Franke, W. Müller, Exp. Tech. Phys. 27 (1979) 13.
[7] I.A. Glavatskikh, V.S. Kortov, H.-J. Fitting, J. Appl. Phys. 89 (2001) 440.
[8] X. Meyza, D. Goeuriot, C. Guerret-Piécourt, D. Tréheux, H.-J. Fitting, J. Appl. Phys. 94 (2003) 5384.
[9] M. Touzin, D. Goeuriot, C. Guerret-Piécourt, D. Juvé, D. Tréheux, H.-J. Fitting, J. Appl. Phys. 99 (2006) 114110.
[10] N. Cornet, D. Goeuriot, C. Guerret-Piécourt, D. Juvé, D. Tréheux, M. Touzin, H.-J. Fitting, J. Appl. Phys. 103 (2008) 064110-1–13.
[11] H.-J. Fitting, N. Cornet, Roushdey Salh, C. Guerret-Piécourt, D. Goeuriot, A. von Czarnowski, J. Electron Spectros. Relat. Phenom. 159 (2006) 46.
[12] J.J. O'Dwyer, The Theory of Electrical Conduction and Breakdown in Solid Dielectrics, Clarendon Press, Oxford, 1973.